JOURNAL OF PROPULSION AND POWER
Vol. 11, No. 6, November–December 1995

Laminar Flow Rotor for a Radial Inflow Turbine

I. Huntsman* and H. P. Hodson†
University of Cambridge, Cambridge CB3 0DY, England, United Kingdom

The state of the boundary layers on the blade surfaces of the rotor of a radial inflow turbine has been investigated using surface-mounted hot-film anemometers. The boundary layers are shown to be laminar or intermittently turbulent at the design flow condition. This is despite the fact that the Reynolds number is relatively high and conventional two-dimensional numerical techniques predict transition at about 20% surface length. The boundary layer does not become fully turbulent because there is strong secondary flow and large acceleration of the flow close to the surface. Surface pressure distributions and an inviscid prediction method are used to assist in the explanation for the state of the boundary layers.

Nomenclature

b = blade span
E = output voltage from anemometer bridge
p = pressure
p^* = reduced static pressure, $p - \frac{1}{2}\rho U^2$
Re = Reynolds number
s = surface length of rotor blade
t' = time nondimensionalized by stator wake passing period
U = blade speed
V = absolute velocity
W = relative velocity
η_{TT} = total–total efficiency
ν = kinematic viscosity
ρ = density
τ_w = blade surface shear stress
Ω = rotational speed

Subscripts
is = reference to isentropic conditions
m = meridional coordinate
mid = midspan position
r = radial coordinate
rel = conditions in the relative frame of reference
x = axial coordinate
y = transformed tangential coordinate
θ = tangential direction
0 = zero flow conditions
1 = stator inlet
2 = stator exit
3 = rotor inlet
4 = rotor exit

Introduction

RADIAL inflow turbines offer several advantages for use in small turboshaft applications when compared with axial turbines for the same duty. This is because the radial inflow turbine offers greater work extraction per stage at comparable or higher efficiencies, increased ruggedness, lower costs of manufacture, and improved packaging when used in conjunction with a reversed flow combustor.

At present, the performance of radial turbines at the design point is predicted using methods based upon correlations. This is because there is little information available regarding the details of the sources of loss in radial inflow turbines, whatever the operating condition. This article is concerned with the nature of the flow close to the blade surfaces of the rotor of a radial inflow turbine at the design flow condition.

The works of Benson et al.,[1] Ariga et al.,[2] and Kitson et al.[3] provide measurements and visualizations of the complex flow patterns that exist, in the region of the inlet to the rotor, at design and off-design flow conditions. In addition, the work of Huntsman and Hodson[4] shows the development of the boundary layer over the first 17% of the blade surfaces of the rotor of a radial inflow turbine, at midspan, using surface-mounted hot-film anemometers. In these references only the flow path near the leading edge of a rotor blade was considered. The remainder of the flow path has not been measured and reported in the open literature. It is believed that only through the advancement of the understanding of the physical processes that govern the flow of fluid through the rotor, that significant improvements in the efficiency or power-to-weight ratio can be achieved in radial inflow turbines.

The flow close to the rotor blade surfaces has been investigated at the design flow condition by determining the pressure distribution around the rotor blades and by flow visualization. Flow visualization data have already been presented and discussed by Huntsman et al.[5] It is presented in this article as Fig. 1. The black marks on the white blade surface give an indication of the direction of the flow close to the blade surface. The secondary flow on both blade surfaces may be observed to be highly three dimensional. In this article, the state of the boundary layers has been examined using surface-mounted hot-film anemometers that were located over the entire length of the blade surfaces of the rotor. The experi-

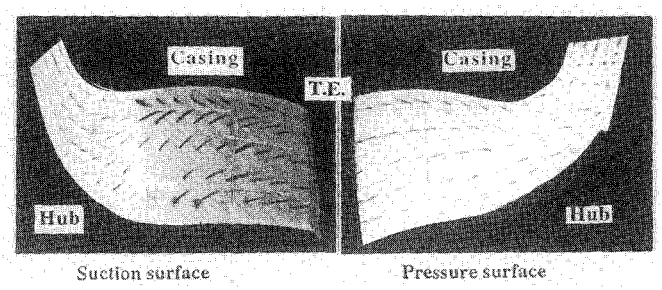

Fig. 1 Flow visualization at the surfaces of a rotor blade.[5]

Presented as Paper 93-1796 at the AIAA/SAE/ASME/ASEE 29th Joint Propulsion Conference and Exhibit, Monterey, CA, June 28–30, 1993; received Aug. 14, 1993; revision received Oct. 24, 1994; accepted for publication Oct. 28, 1994.

*Rolls–Royce Senior Research Fellow, Whittle Laboratory, Madingley Road; currently Lecturer, Department of Mechanical Engineering, University of Canterbury, Christchurch, New Zealand. Member AIAA.

†Lecturer. Member AIAA.

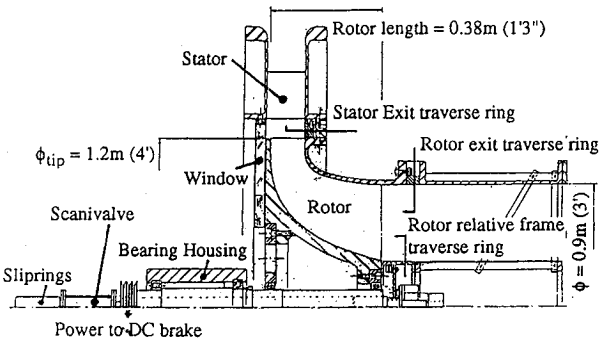

Fig. 2 Layout of the test rig.

mental data in the region close to the rotor leading edge have been interpreted with the aid of an inviscid, incompressible panel method based on the method of Hess and Smith.[6]

Experimental Arrangement

The radial turbine used for the present investigation has been described by Huntsman et al.[5] A general assembly drawing of the turbine rig is shown in Fig. 2. This turbine is a low-speed model of a Rolls–Royce development turbine. Some important parameters for the model turbine are presented in Table 1.

The rig operates as an open loop wind tunnel drawing air from the atmosphere through an axisymmetric bellmouth into the model turbine. A filter surrounds the bellmouth. A volute is not used in this machine, but there are 23 radial flow stator blades that deflect the air through an angle of 72 deg. The flow enters the rotor at an angle in the relative frame of −18 deg. The air leaves the rotor predominantly in the axial direction and travels along a circular exhaust duct through a honeycomb flow straightener to a sliding, axisymmetric throttle and the suction fan.

Slip rings are used to carry the control and monitoring signals to the on-rotor Scanivalve and to the hot-film anemometers on the rotor blade surfaces.

At the rotor exit, there is a rotating radial–circumferential traverse system that enables the acquisition of data from the relative frame of reference. The movement of the stepper motors was monitored by optical encoders mounted on the shafts of the motors. Boundary-layer traverses have been undertaken in the relative frame using a flattened pitot probe.

Surface-Mounted Hot-Film Anemometers

In the previous study, on a different turbine, Huntsman and Hodson[4] placed hot-film anemometers over the first 17% of the midspan of the blade surfaces. For the present turbine it was possible to place hot-film anemometers over the entire surface of a rotor blade. Results will be presented from an array of gauges that were wrapped around the leading edge at midspan and bonded directly to the blade surface. Each sensor was 1 × 0.1 mm in size and the thickness of the substrate and glue is typically about 0.05 mm. The electrical leads were routed along the blade surface to the hub corner and then along the hub corner to the rotor exit. The distance between adjacent gauges corresponded to 0.9% of the surface length. Downstream of this region a coarse resolution was used. The hot-film gauges were placed at 20, 50, and 80% span.

The hot-film anemometer sensors were operated at constant temperature. The temperature profile through the boundary layer, generated by the hot-film anemometer, is similar to the velocity profile of the boundary layer (cf. Reynolds analogy). The relationship between the rate of heat transfer to the fluid and the wall shear stress[7] is of the form:

$$\tau_w \propto [(E^2 - A^2)/\Delta T]^3$$

Table 1 Leading parameters for the turbine at the design flow condition

Stator exit radius, 677 mm
Stator radial chord, c_{radial}, 165 mm
Rotor inlet radius, 609 mm
Rotor exit rms radius, 336 mm
Rotor inlet blade span, 133 mm
Rotor exit blade span, 278 mm
Rotational speed, 450 rpm
Mass flow rate, 5.4 kg/s
Number of stator blades, 23
Number of rotor blades, 14
$Re_{\text{Hiett and Johnston}}$, $Re_{HJ} = U_3 b_3/\nu_1$, 2.6×10^5
$Re_{\text{Stator}}(c_{radial}V_2/\nu_2)$, 2.8×10^5
Rotor $Re_{\text{surface length}}$, $Re_s = W_{4\,mid} s_{mid}/\nu_{4\,mid}$, 1.0×10^6
Design specific speed, N_s, 0.61
Stator inlet angle (from radial), 0 deg
Stator exit angle, 72 deg
Rotor inlet angle, −18.4 deg
Rotor exit angle—hub, −51 deg
Rotor exit angle—rms radius, −66 deg
Rotor exit angle—casing, −72 deg

The term E is the bridge output voltage, the constant A represents the heat lost from the sensor to the substrate, and ΔT is the temperature difference between the hot-film sensor and the flow. In some of the previous low-speed work at the Whittle Laboratory, individual hot-film gauges were calibrated (see, e.g., Ref. 8). In the present case, however, the calibration of an array of gauges would have been both difficult and time-consuming. It was decided, therefore, to adopt a similar procedure to that described by Hodson.[9] The constant A, in the preceding equation, is assumed to be approximately equal to the bridge output voltage measured under zero flow conditions. The temperature difference ΔT is assumed to be related to the square of the voltage measured at zero flow conditions. In practice, this means that the data is reduced to the form:

$$\tau_w \propto [E^2 - E_0^2)/E_0^2]^3 \quad (1)$$

The output signal from the anemometer was cut off using a 10-kHz low-pass filter before being digitized at a rate of 20 kHz. The upper frequency limit to the response of the hot-film sensors was determined using a square wave input to the Whetstone bridge and was found to be of the order of 25 kHz.

Further details on the usage of hot-film anemometers were given by Hodson.[9]

Surface Pressure and Velocity Distributions

The flow path through the rotor is highly three dimensional, and so spanwise variations in pressure are significant. There are, therefore, five spanwise tappings in each of the 42 pressure lines that run beneath the surface of the instrumented rotor blade. Consequently, the variation of pressure along the span can be measured with good resolution. During the experiments the four tappings not under investigation were sealed using adhesive tape. The 42 pressure lines from around the blade surface were all connected to the on-rotor Scanivalve pressure switch and transducer arrangement (see Fig. 2). The measured pressures were corrected for the variation of pressure due to rotation and the change of radius from the tapping to the Scanivalve. The stagnation pressure at the inlet to the rig p_{01} was used as the back pressure for the transducer. The electrical connections between the rotating and the stationary frame were made via slip rings.

The data obtained from the blade surface pressure tappings will be presented in the form of isentropic surface velocities. The isentropic velocities are determined from the use of the

rotational form of Bernoulli's equation and Euler's work equation:

$$p + \tfrac{1}{2}\rho W^2 - \tfrac{1}{2}\rho U^2 = \text{const} = p_{03} - \rho U_3 V_{\theta 3}$$

The stagnation pressure at the inlet to the rotor p_{03} was calculated from the measured inlet stagnation pressure p_{01} and the mass-averaged loss of stagnation pressure at the exit from the stator blades ($\overline{Y_{p\,\text{stator}}} = 0.021$). The isentropic velocities are nondimensionalized by dividing by the radial component of the velocity at the rotor inlet V_{r3} (or W_{r3}).

Data will be presented as contours on a meridional ($r - x$) projection of the blade. Data will also be presented in graphical form where the velocity at a particular spanwise location is plotted against surface distance. Although this is a convenient form of presentation it must be emphasized that the flow of fluid through the rotor of a radial turbine is highly three dimensional. The graphs at constant span do not, therefore, represent flow along a streamline, but merely the distribution of the isentropic velocity along a particular line on the blade surface.

Numerical Predictions

Inviscid Flowfield

An accurate prediction of the velocity distribution near the leading edge of the rotor assists in the understanding of the pressure gradients that the boundary-layer fluid is subjected to. It is common to analyze the flow through turbomachinery blade rows using three-dimensional time-marching techniques (see, e.g., Ref. 3). The time-marching prediction methods available to the authors[10,11] use H-type meshes. With this type of mesh it is difficult to obtain adequate resolution of the flowfield at the leading edge of the rotor of a radial turbine. Indeed, the predictions presented by Kitson et al.[3] (using the Dawes[11] code) were compromised by the significant entropy change that occurred due to numerical viscosity acting in the region near the leading edge of the rotor where the mesh was skewed. It was decided, therefore, to develop a numerical method to enable the accurate prediction of the flowfield near the leading edge of the rotor. The present radial inflow turbine operates with incompressible flow. In addition, the rotor is of simple radial element construction, and so, in the locality of the leading edge, the blades are purely radial. An incompressible two-dimensional numerical method has, therefore, been developed.

An idealized two-dimensional panel method based on the method proposed by Hess and Smith[6] was discussed previously by Huntsman and Hodson.[4] In this method the governing equations are solved in integral form. Figure 3 shows that the blade surface is divided into many small lengths that are known as "panels." A uniform source strength is assumed to act over the length of each panel. By applying a conservation of mass condition and a boundary condition of zero velocity normal to the center of each panel the potential field due to the blade is simulated. The blade lift is calculated by placing a uniform distribution of point vortices along every panel. The magnitude of the point vortices is determined by applying the Kutta condition at the trailing edge of the blade. The formulation for the Kutta condition is similar to that suggested by Wilkinson[12] and consists of equating the velocity parallel to the blade surface at the nodes on either side of the trailing edge.

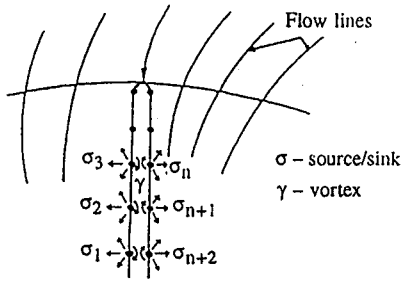

Fig. 3 Outline of the panel method.

The inviscid method has been extended to predict the flow in a blade-to-blade plane for the true meridional blade shape rather than an idealized two-dimensional blade profile. Such an improvement in the method enables more general comparison with the experimental data obtained from the pressure tappings in the rotor blade surfaces.

The governing equations for the conservation of mass and vorticity, in the relative frame of reference, for the flow around the blades are

Conservation of mass

$$\frac{\partial}{\partial \theta}(\rho b W_\theta) + \frac{\partial}{\partial m}(\rho r b W_m) = 0$$

Conservation of vorticity (Kelvin's circulation theorem)

$$\frac{\partial}{\partial m}(r W_\theta) - \frac{\partial}{\partial \theta}(W_m) = -2\Omega r \frac{\mathrm{d}r}{\mathrm{d}m}$$

where m is the meridional distance and the term involving 2Ω is the relative vorticity, the Coriolis effect, due to the change in radius. Changes in the streamtube thickness b are included in the equation for the conservation of mass. The $\mathrm{d}r/\mathrm{d}m$ term allows for the change in the direction of the meridion from radial at inlet to axial at exit. The density ρ in the radial turbine tested in this work is almost constant, but is included in the formulation of the equations for completeness.

Wilkinson[13] transformed the governing equations into the cascade plane using the transformation:

$$y = \theta, \qquad x = \int_{m_{\text{le}}}^{m} \frac{\mathrm{d}m}{r}$$

where m_{le} is the meridional distance at the leading edge of the blade. When the blades are radial $\mathrm{d}m$ is equal to $\mathrm{d}r$. For radial blades this transformation is equivalent to using the familiar $f = \log z$ conformal mapping from the circular ($r - \theta$) plane to the cascade ($x - y$) plane. In the transformed plane the velocities are represented by

$$W_x = \rho r b W_m, \qquad W_y = \rho r b W_\theta$$

The governing equations, therefore, reduce to

Conservation of mass

$$\frac{\partial}{\partial y}(W_y) + \frac{\partial}{\partial x}(W_x) = 0$$

Conservation of vorticity

$$\frac{\partial}{\partial x}(W_y) - \frac{\partial}{\partial y}(W_x) = \frac{W_{y\,\text{est}}}{\rho b}\frac{\mathrm{d}}{\mathrm{d}x}(\rho b) - 2\Omega \rho b r \frac{\mathrm{d}r}{\mathrm{d}x}$$

$W_{y\,\text{est}}/\rho b$ is an estimate of the value of the angular momentum in the relative frame rW_θ, which is obtained by assuming that the flow follows the camberline of the blade. A one-dimensional calculation using the passage geometry is all that is required to estimate the flow turning and flow area at every meridional point. Alternatively, a throughflow analysis may be used to calculate values for the angular momentum and the flow area. The term in the equation for the conservation of vorticity that involves the estimate for the angular momentum in the relative frame is the main approximation in the equations. This term is the only significant change that must be made to the existing algorithm that predicts the flow around

an idealized two-dimensional blade profile. McFarland's work[14] shows that slight changes in the approximation for $W_{y\,est}$ have little effect on the predicted solution.

By accepting the compromise of making the solution approximate, the effects of stream sheet thickness and nonradial direction of the meridion have been included into the prediction method.

Comparison with Experimental Data

A convenient demonstration of the applicability of the extended panel method is to compare the predicted with the measured velocity distribution for the rotor blades from the radial turbine. Figure 4 shows the comparison of the isentropic velocity distributions for the midspan of the rotor blades at the design flow condition. The overspeed at the leading edge of both surfaces is resolved well. The predicted velocities on the suction surface compare well with the measured velocities. It is possible, therefore, to make general suggestions concerning the boundary-layer behavior on the suction surface from the predicted results (which are for inviscid flow). After the overspeed at the leading edge the flow does not decelerate at any point along the midspan of the suction surface. It would be anticipated, therefore, that the boundary layer does not separate from the suction surface downstream of the leading-edge region. It must be remembered, however, that the results at midspan do not correspond to measurements along a streamline.

Near the leading edge of the pressure surface the difference between the measurement and prediction shows that the deceleration after the overspeed causes the boundary layer to separate from the blade surface. Reattachment occurs at about 3% surface length (see Fig. 4). When the inviscid velocity distribution is used as the input data for Thwaites' method, the separation of the boundary layer on the pressure surface is predicted. The decrease in velocity at 54% surface length is well-resolved by the panel method. Unfortunately, the increase in velocity from 54% surface length to the trailing edge is not accurately predicted.

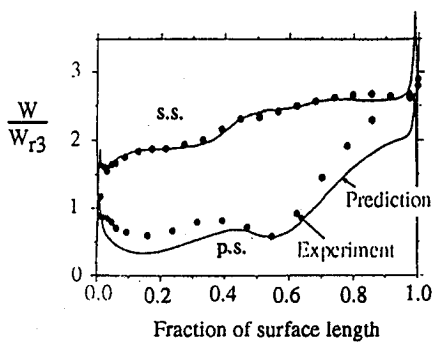

Fig. 4 Measured and predicted velocity distributions at the design flow condition for the midspan of a rotor blade.

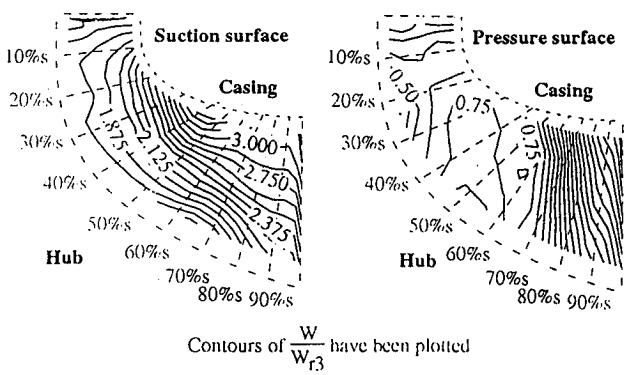

Fig. 5 Isentropic velocity distribution on the surfaces of a rotor blade at the design flow condition.

Results and Discussion

Blade Surface Pressure and Velocity Distributions

Figure 4 shows the isentropic velocity distribution for the midspan of the rotor blades at the design flow condition. Meridional contour plots of isentropic velocity for the suction and pressure surfaces are shown in Fig. 5.

Suction Surface

One of the main features to note from Fig. 4 is that the velocity increases from just after the overspeed at the leading edge to the trailing edge, on the suction surface. The ratio of the velocity at the exit from the rotor to that at the inlet to the rotor is 2.7. The value chosen by Rohlik,[15] and used in many subsequent designs, was 2.0. The increase in the velocity ratio across the rotor is mainly a result of the negative swirl, in the stationary frame, of -26 deg, which is present at the rotor exit. It was necessary to have negative swirl at the rotor exit to increase the power output from the baseline turbine from which the present rig was modeled. Increasing velocity with surface length along the midspan is expected to provide favorable conditions for boundary-layer development. High velocity at the rotor exit reduces the total-static efficiency and, consequently, increases the potential advantages of using a diffuser. The total-static efficiency for the present turbine, which does not have a diffuser, is 0.88 ± 0.03.

Figure 5 shows that there is initially a rapid acceleration of the flow at the leading edge of the suction surface that is almost two dimensional (i.e., follows the meridional coordinate). Beyond about 7% surface length, however, it may be observed that the component of the gradient of the contours in the spanwise direction is significant. The low momentum flow in the boundary layer on the suction surface responds to the gradient of the reduced static pressure, and as a result secondary flow occurs towards the casing. The isentropic form of Euler's work equation can be used to show that contours of reduced static pressure follow the same path as the contours of isentropic velocity. The flow downstream of 7% surface distance cannot be considered to be subjected to two-dimensional forces only. The flow visualization of Fig. 1 shows, however, that the fluid in the boundary layer does not respond to the spanwise component of the force on the flow until about 20% surface length. The streamline curvature in the meridional plane, which is a consequence of the flow path turning from the radial direction towards the axial, causes the pressure gradient towards the casing.

As the surface distance increases further, the meridional curvature is reduced, but there is now an appreciable component of velocity in the circumferential direction (due to blade curvature). The cross-product of the circumferential velocity with the rotational speed leads to Coriolis acceleration and, consequently, a force on the flow that acts on the low momentum fluid in the blade surface boundary layers to cause secondary flow in the radial direction.

At the rotor exit there is nonuniform spanwise loading so that shed vorticity is present. The nonuniform loading distribution creates a component of the gradient of the reduced static pressure, and hence, the isentropic velocity, in the spanwise direction, at the trailing edge.

Pressure Surface

Figure 5 shows that the nature of the flow along the pressure surface is quite different to that observed close to the suction surface. The most notable difference is that the direction of the contours of constant velocity are aligned closer to the spanwise direction. This suggests that over much of the blade surface the flow in the boundary layer is not as strongly three dimensional. Near the leading edge of the pressure surface

the velocity is constant, suggesting the presence of a small separation bubble (this may be observed on Fig. 4). The velocity remains low to about 60% surface length. From this point there is a rapid acceleration to the trailing edge. Between 15 and 50% surface length there is a gradient of isentropic velocity in the spanwise direction. This is where, in the meridional plane, the radius of curvature is smallest. As a consequence there is secondary flow towards the low reduced static pressure at the casing. The secondary flow may be observed in the flow visualization that was presented in Fig. 1. Further downstream the loading distribution along the span is nonuniform. At the rotor exit the shed vorticity counteracts the secondary flow induced by the meridional curvature and Coriolis acceleration. The secondary flow is, therefore, towards the hub.

Development of the Blade Surface Boundary Layers

The signals from the hot-film anemometers have been plotted according to Eq. (1). The resulting output is approximately proportional to the shear stress at the blade surface. The units are arbitrary. The time t is measured relative to a fixed angular point on the stator blade assembly. In each of the traces shown the time abscissa has been nondimensionalized with respect to the time taken for the rotor to pass one stator blade passage T_s. The nondimensionalized time t' is therefore equal to t/T_s. The percentage of the surface length from the leading edge is shown next to each output trace.

Measurements close to the leading edge of each blade surface were obtained by wrapping an array of hot film anemometers around the leading edge. The variation in resistance between the elements of this array was found to be small. In addition, since all the hot films had a common substrate, the relationship between the heat loss to the substrate and the zero flow voltage was similar for all the gauge elements. These two factors imply that the constant of proportionality between the output signal and the shear stress was almost of the same magnitude for all the gauges. Consequently, the magnitude of the signal may be used to infer changes in the properties of the boundary layer.

Unfortunately, the array of hot-film anemometers only covered a small percentage of the blade surface length (about 9%) and could not be used near the hub and casing. It was decided, therefore, to use individual gauges for the remainder of the blade surface. These hot-film anemometers have slightly different substrate properties and varying gauge resistance. The constant of proportionality between the zero flow voltage and the heat loss to the substrate is of different magnitude for these individual hot-film anemometers. It is not appropriate, therefore, to place as significant an emphasis on the magnitude of the output from the different anemometers. Large variations in magnitude are, however, still indicative of significant change in the nature of the boundary layer. The data is, therefore, presented in a nondimensional form. The signal level was divided by the time mean of the signal.

Suction Surface

Close to the Leading Edge

Figure 6 shows a few of the results that were obtained from the array of hot-film anemometers that were wrapped around the leading edge. The last result, at 14% surface distance, was obtained by placing a separate hot-film anemometer downstream of the leading-edge arrangement. The signals all display the high magnitude associated with the shear stress found in attached boundary layers. In addition, only low frequency disturbances are present in the boundary layer. The boundary layer is, therefore, attached and in a laminar state over this early portion of the rotor. The wakes shed from the upstream stator blades are not easily distinguished in the data presented. The trailing-edge thickness and the momentum deficit in the boundary layer are both small for the stator

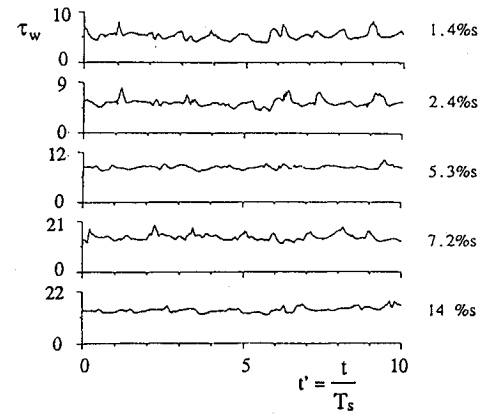

Fig. 6 Hot-film anemometer signals from the midspan of the suction surface, near the leading edge, at the design flow condition.

blades (at midspan the stagnation pressure loss coefficient is 0.014). It is unlikely, therefore, that the wakes shed from the upstream blades will have a significant effect on the development of the boundary layer on the first portion of the rotor blades.

In order to gain an appreciation of the point at which transition from a laminar to a turbulent boundary layer is to be expected, the Herbert and Calvert[16] integral method was applied to the measured and predicted velocity distributions at the midspan. The prediction method is similar to Thwaites' method when the boundary layer is laminar. The transition criterion used is that transition to a turbulent boundary layer occurs when the Reynolds number based on the momentum thickness Re_θ has a value of 163 (this is in accordance with the correlations of Abu-Ghannan and Shaw[17]). Hodson et al.[18] suggest that transition begins to occur when Re_θ is between 90 and 250.

Although this is a somewhat crude method for finding the point of the start of transition it is only used to indicate the region where transition might begin. There is only a small extent of two-dimensional boundary-layer development on the rotor blade. The prediction method indicates that transition is likely to begin to occur at around 17% surface length. The data from the hot-film anemometers that is presented here is, therefore, in agreement with the prediction of a stable, laminar boundary layer over the first 14% of the surface length.

Boundary-Layer Development Downstream of the Leading Edge

It was shown in the previous section that the boundary layer on the suction surface, at midspan, at the design flow condition, is laminar up to 14% surface distance. Gauges were placed at three spanwise positions and up to 18 meridional positions over the remainder of the blade surface. A selection of the data will be presented here.

Midspan Results

Figure 7 presents the output signals from seven hot-film anemometers.

The anemometer positioned at 16% surface length shows the low-frequency disturbances that were observed earlier in the boundary layer close to the leading edge. In addition, e.g., at $t' = 7.8$, there are a few large scale events that could be regions of coalesced turbulent spots. The boundary layer is essentially laminar at 16% surface length. At 29% surface length the boundary layer is more disturbed, a greater number of large amplitude fluctuations are present. Turbulent regions may now be observed in the signal, e.g., at $t' = 2.5$. Over the remainder of the signal the only fluctuations present are at the low frequencies typical of a laminar boundary layer subjected to disturbances in the freestream. The conclusion is that at 29% surface length the boundary layer is essentially

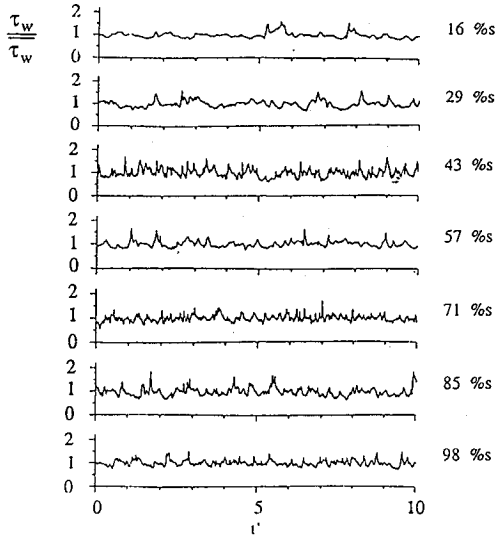

Fig. 7 Hot-film anemometer signals from the midspan of the suction surface at the design flow condition.

laminar, but that transition is just beginning to occur. The intermittency will be low.

At 43% surface distance the frequency of the fluctuations is much higher than those present at 29% surface length. Regions of turbulent flow may now be observed at some points in the signal, e.g., between $t' = 7.2$ and $t' = 8.2$. A turbulent spot or a region of coalesced turbulent spots may be recognized, because in this region the level of the signal is significantly greater than the laminar level. The frequency of the fluctuations is also high due to the turbulent eddies present within the "spot." Indeed, for a significant proportion of the output at this location the turbulent spots have almost merged to form a turbulent boundary layer. The intermittency at this position is high, in the region of 50%.

After analysis of the boundary-layer state at 43% surface distance it would be relatively straightforward (and erroneous) to conclude that the boundary layer at midspan on the suction surface was turbulent from about 43% surface length for this blade. The Reynolds number in the form presented by Hiett and Johnston[19]:

$$Re_{\text{Hiett\&Johnston}} = U_3 b_3/\nu_1$$

has a value of 2.6×10^5. When based on the surface length:

$$Re_{\text{surface length}} = W_{4\,\text{mid}} s_{\text{mid}}/\nu_{4\,\text{mid}}$$

the measured Reynolds number has a value of 1×10^6 for this turbine. The high magnitude of both the Reynolds numbers suggests that turbulent boundary layers are expected to develop from a point near the leading edge of the rotor, depending on the form of the velocity distribution. Indeed, the previously mentioned boundary-layer prediction method gave the result that transition would be at 17% surface length. Attention must be drawn to the data from the remainder of the suction surface, however, before any conclusions concerning the state of the boundary layer can be postulated.

At 57% surface length the idea of a turbulent boundary layer is challenged by the output from the hot-film anemometer. Although there are fluctuations present in the boundary layer the disturbances are mainly of a low-frequency nature. A general comparison of the output at 43, 57, and 71% surface length shows the very different nature of the boundary layer at 57% surface length. The low frequency of the fluctuations suggests that the boundary layer is still of a laminar character. The boundary layer would be termed a "disturbed" laminar boundary layer because a "true" laminar boundary layer displays none of the fluctuations seen in the output from this anemometer.

One of the reasons for the change in the boundary-layer state between 43% surface length and 57% surface length is linked to the spanwise component of the gradient of the isentropic velocity (shown in Fig. 5). As a result of this gradient the fluid in the boundary layer close to the blade surface moves towards the casing as shown in Fig. 1. A "new" boundary layer forms close to the hub to take the place of that which formed the secondary flow. The low momentum fluid at 57% surface distance will not have passed through the same pressure field as that at 43% surface distance. The flow visualization in Fig. 1 highlights the strong secondary flow present over the latter portion of the rotor blades.

Another important factor that must be considered is the nondimensional acceleration parameter k which is expressed as

$$k = \frac{\nu}{W^2}\frac{\partial W}{\partial s}$$

or for three-dimensional flow

$$k = (\nu/W^2)\nabla(W) \tag{2}$$

It has been shown empirically[20] that in cases of decreasing reduced static pressure in the freestream, that turbulent boundary layers tend to relaminarize if the acceleration parameter has a value greater than 3×10^{-6}. In the present case the acceleration seems not to relaminarize a turbulent boundary layer, but prevents a laminar boundary layer from becoming fully turbulent. However, as shown in the output of the anemometer at 57%s there are still fluctuations present in the boundary layer. This leads to the description of the boundary layer as disturbed. Analysis of the gradient of isentropic velocity on the suction surface that was presented in Fig. 5 leads to the values of the acceleration parameter shown in Fig. 8. The shaded regions on Fig. 8 represent areas where the streamwise component of the acceleration parameter is negative. The contours represent the magnitude of the acceleration parameter (i.e., the combined streamwise and spanwise acceleration). The maximum value for the magnitude of the acceleration parameter on the suction surface is close to 7×10^{-6}. More common values range from 2–3.5 $\times 10^{-6}$ (see Fig. 8). It is likely, therefore, that relaminarization is possible over much of the suction surface. The acceleration parameter reduces to just above zero close to the trailing edge. It is possible that the boundary layer could have high intermittency, or be fully turbulent, close to the trailing edge of the blade.

At 71% surface length the hot-film data of Fig. 7 again show the presence of high-frequency fluctuations. This is consistent with an intermittent turbulent boundary layer. There are still regions where the fluctuations are at a lower fre-

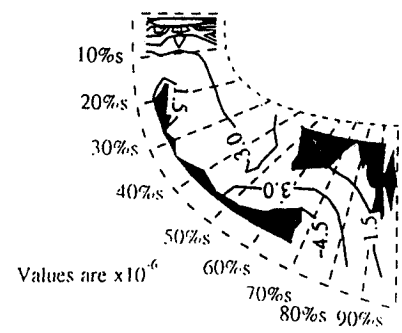

Negative streamwise acceleration has been shaded

Fig. 8 Contours of acceleration parameter [Eq. (2)] on the suction surface at the design flow condition.

Table 2 Boundary-layer parameters measured at the midspan at the rotor exit using a flattened pitot probe

	Suction surface	Pressure surface
Displacement thickness, δ^*	0.56 mm	0.32 mm
Momentum thickness, θ	0.37 mm	0.16 mm
Shape factor, H	1.52	2.08
Intermittency (based on H), γ	0.8	0.1
Blade pitch at exit (midspan)	140 mm	140 mm

quency, and a higher amplitude, than would be expected for a turbulent boundary layer. The output at 85% surface length has distinct turbulent regions present (e.g., $t' = 1.8$ and at $t' = 5.5$), and is, therefore, typical of transition within a disturbed laminar boundary layer. The other disturbances present are low-frequency (or, large length scale, of the order of the pitch of a stator blade) and not typical of features within a turbulent boundary layer. The last output signal (at 98%s) appears to show regions where turbulent spots are present ($t' = 2.8$ and $t' = 7$), regions where the turbulent spots may have joined to give a turbulent boundary layer ($t' = 4$–5), and regions of lower frequency fluctuations indicative of a disturbed laminar boundary layer ($t' = 0$). It is thought that at 98% surface length the boundary layer is transitional with a high value of intermittency.

It is worth noting at this point that boundary-layer measurements obtained at the midspan at the rotor exit using a flattened pitot probe indicated that the thickness of the boundary layer at the rotor exit was 5 mm. The boundary-layer parameters are presented in Table 2. The shape factor was 1.52. The correlations of Abu-Ghannan and Shaw[17] suggest that this value corresponds to an intermittency of 0.8. The above interpretation of the data from the hot-film anemometer is, thus, not contrary to the results obtained from the boundary-layer traverse. The low value for the displacement and momentum thicknesses is in keeping with the high efficiency of this turbine ($\eta_{TT} = 0.93 \pm 0.03$). These low values for the boundary-layer parameters arise partly because over much of the blade surface the boundary layer is laminar, or has low intermittency. At the rotor exit the boundary layer did not originate at the rotor leading edge. The boundary layer at the rotor exit at midspan formed at the hub a significant distance from the leading edge and then moved under the influence of the reduced static pressure field to the measurement point. The boundary-layer fluid that arrives at the trailing edge of the rotor at midspan is unlikely to have been subjected to an adverse gradient of reduced static pressure.

Results at 20% Span

The output from several hot-film anemometers placed at 20% span are shown in Fig. 9. The results from the anemometer at 16% surface length shows occasional turbulent spots within the low-frequency disturbances that are associated with a disturbed laminar boundary layer.

At 29% surface length the fluctuations within the boundary layer show components at higher frequency, which suggests that the boundary layer is beginning to undergo transition. The prediction method of Herbert and Calvert again predicts that transition to a turbulent boundary layer occurs at about 17% surface length.

The remainder of the data presented in Fig. 9 does not show an increased level of disturbance relative to the data at 29% surface length. In fact, only low-frequency disturbances are present in the data from 43–98% surface length. These low-frequency (large length scale) fluctuations are typical of those observed in the results at midspan, but are much easier to interpret because the data at 20% span is not confused by the boundary layer beginning to become transitional.

The output at 85% surface length is particularly free from disturbances. Turbulent spots are probably just beginning to develop in the boundary layer at 98% surface length. Most of the disturbances are, however, more characteristic of the low-frequency oscillations that can develop in a laminar boundary layer.

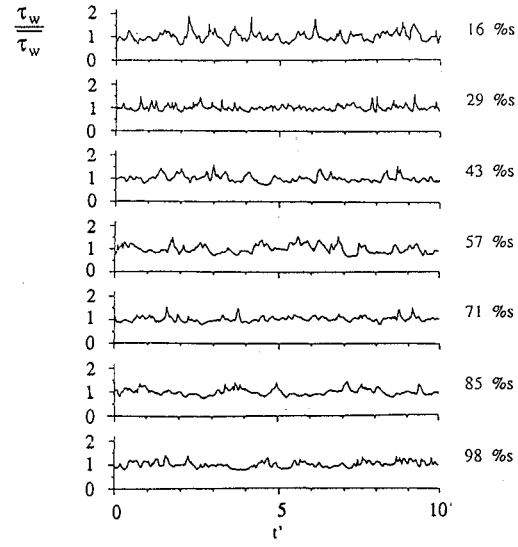

Fig. 9 Hot-film anemometer signals at 20% span on the suction surface at the design flow condition.

The reason for the decrease in the amplitude and frequency of the fluctuations within the boundary layer, from 16% surface length to the trailing edge, is the component of the gradient of the reduced static pressure in the spanwise direction that was mentioned previously. The measurement at 29% surface length is thought to correspond to the maximum streamwise extent, at this spanwise location, of the boundary-layer fluid that originated at the rotor leading edge. Elsewhere, the boundary layer at 20% span originated from the hub of the blade at a streamwise position away from the leading edge. The boundary layer is still of a laminar nature at 20% span simply because the fluid has only moved over a short length of surface.

Results at 80% Span

To complement the data shown previously, Fig. 10 displays the output from the same streamwise positions that were shown earlier, but at 80% span. As before, in the region before significant development of spanwise secondary flow, the boundary layer is highly disturbed with a few turbulent spots present. Turbulent spots may be observed in the data at 16% surface distance at $t' = 7.5$ and at 29% surface length when $t' = 2$. These data are similar to those presented at both 20% span and midspan. This is not surprising given that the flow visualization presented in Fig. 1 shows that little spanwise secondary flow occurs in the first 20% of the surface length.

At 43% surface distance many turbulent spots are present in the boundary layer. There are many positive spikes in the data (i.e., high positive skew), and the amplitude of the fluctuations is of the same order as the mean signal level. The boundary layer is, therefore, intermittently turbulent at this position. The amplitude of the turbulent fluctuations in a fully turbulent boundary layer is generally much smaller than the mean signal level. The reason for such a large number of turbulent spots at 43% surface length becomes apparent after consideration of the variation of the acceleration parameter at the blade surface near this spanwise location (Fig. 8). Deceleration of the flow, in the streamwise direction, occurs near 43% surface length. The spanwise component of the acceleration parameter near 80% span, 43% surface length is small. The value of Re_θ predicted by Thwaites' method (for a laminar boundary layer) at 43% surface length is 300. The boundary layer at 43% surface distance will be sufficiently well-estab-

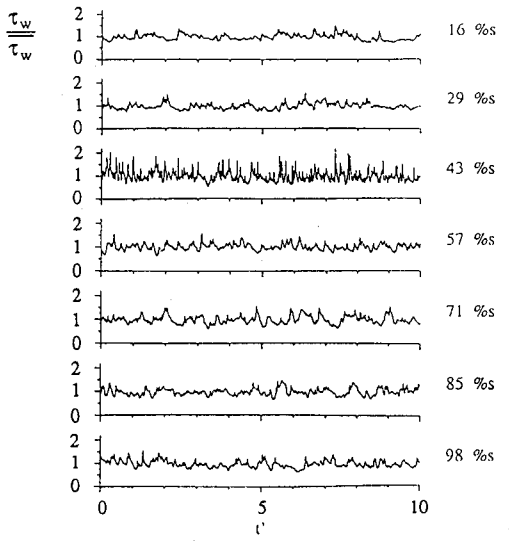

Fig. 10 Hot-film anemometer signals at 80% span on the suction surface at the design flow condition.

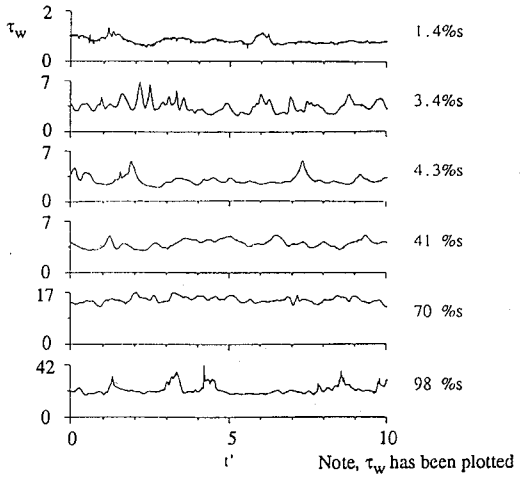

Fig. 11 Hot-film anemometer signals at midspan on the pressure surface for the design flow condition.

lished for transition to begin if subjected to either constant or increasing reduced static pressure. At 46% surface length the acceleration parameter k in the streamwise direction (i.e., neglecting the spanwise component) is -0.6×10^{-6}. Before the maximum in the velocity the streamwise component of the acceleration parameter is 2.5×10^{-6}. Mayle[21] reviewed the data on transition obtained by several authors. He showed that changing the acceleration parameter over a range from 0.75×10^{-6} to -0.6×10^{-6} caused the rate of formation of turbulent spots to increase by a factor of 10. The high degree of intermittency in the signal from the hot-film anemometer is mainly a result of the increase in the formation rate of turbulent spots that occurs in a decelerating flow.

From 57 to 98% surface length the boundary layer is highly disturbed, but the high-frequency fluctuations are no longer present. This suggests that the boundary layer is again laminar, although there are still the occasional large-scale disturbances and a few turbulent spots. The boundary-layer fluid at 43% surface length continued moving in the spanwise direction until it was entrained into the vortex that forms near the casing. The boundary-layer fluid arriving at the 80% span position from 57 to 98% surface distance is not subjected to the pressure rise observed at 43% surface length. As a result the output from the anemometers still displays the characteristics of a disturbed laminar boundary layer.

Pressure Surface

Further reference to the midspan velocity distribution (Fig. 4) shows that low velocities are present over the first 54% of the surface distance of the pressure surface. The strong acceleration towards the trailing edge results in a value of the streamwise acceleration parameter well in excess of 3×10^{-6} (typically between 4×10^{-6} and 10×10^{-6}). This strong acceleration suggests that a significant part of the pressure surface will always have attached, laminar boundary layers. Close to the trailing edge the acceleration parameter reduces to zero, and so it is possible that transition may begin to occur close to the trailing edge. The sharp fall in velocity at 54% surface distance is due to a region of high curvature in the blade profile.

With low velocity over the first 54% of the length of the pressure surface the shear stress at the blade surface is low. It is difficult, therefore, to distinguish between the low shear stress present at the blade surface when the boundary layer is separated and the low shear due to low freestream velocity. For this reason the results from the hot-film anemometers near the leading edge must be analyzed carefully before being used to explain the state of the boundary layer.

Figure 11 shows the output from some of the anemometers on the pressure surface at the design flow condition. The first signal at 1.4% surface length has a very low magnitude. There are disturbances present in the boundary layer, but these are superimposed upon a fairly flat baseline. The boundary layer is separated at this position on the blade surface. At 3.4% surface length the signal level has increased, but there are now many high-amplitude disturbances present in the anemometer output. This type of signal is also typical of a separated boundary layer. The high-amplitude, low-frequency fluctuations are due to disturbances in the free shear layer (or the freestream), which convect/diffuse to the blade surface. The higher shear stress observed at this point suggests that the anemometer is positioned close to the point of reattachment. Although the shear stress at 4.3% surface length has not increased from the value at 3.4% surface length, the baseline to the signal is not flat and the fluctuations appear as low-frequency, large-length scale, disturbances. The velocity distribution shown in Fig. 4 indicates that the boundary layer reattaches near this location. A turbulent spot is present in the signal at $t' = 1.6$. The output from the anemometer at 4.3% surface distance indicates nevertheless that the boundary layer is essentially laminar. It is slightly surprising that the boundary layer is not turbulent after reattachment. The reasons for this are not understood. One possible explanation is that the reattachment process is strongly influenced by the three-dimensionality of the flowfield. Another possibility is that the disturbances in the boundary layer that were observed at 3.4 and 4.3% surface length transfer relatively high momentum fluid towards the blade surface, and this aids the reattachment process.

Moving down the blade surface to 41% surface length, the output from the anemometer appears to be similar to that observed at 4.3% surface length. The magnitude of the shear stress is also similar at the two positions. As mentioned earlier there is low velocity on the pressure surface over a substantial portion of the blade. This has the benefit of low loss and provides the opportunity for high loading, providing the boundary layer on the pressure surface remains attached.

At 70% surface length the shear stress is higher than before and there are only low-frequency fluctuations present in the boundary layer. The boundary layer is, therefore, laminar. The increased magnitude of the shear stress is due to the increase in velocity after 54% surface length (see the velocity distribution of Fig. 4). The anemometer output at 98% surface length shows the presence of turbulent spots. At $t' = 3$ and $t' = 4.2$, the shear stress rises sharply and high-frequency fluctuations appear within the boundary layer, the obvious

signs of a single turbulent spot or several coalesced turbulent spots. There are only a small number of turbulent patches present in the signal, and so the intermittency is low. Boundary-layer measurements using a flattened pitot probe provide the results shown in Table 2.

The low value of the intermittency (of 0.1), calculated using the correlations of Abu-Ghannan and Shaw,[17] agrees with the interpretation of the output from the hot-film anemometer at 98% surface distance. The momentum thickness and displacement thickness are both small, so again, it is not surprising that this turbine has a particularly high value of efficiency, even with a small separation bubble near the leading edge of the pressure surface.

The flow visualization presented in Fig. 1 and the contours of isentropic velocity presented in Fig. 5 show that the movement of the low momentum fluid within the boundary layer is almost along the streamwise direction over the range 0–20% surface distance. From 54 to 100% surface length, the inclination of the contours shows that there is only a small component of the gradient of isentropic velocity in the spanwise direction. Since the data from the hot-film anemometers is difficult to interpret in the low-velocity region, and elsewhere the flow is almost two dimensional, only the midspan position has currently been investigated with hot-film anemometers. It is known from the velocity distribution and the flow visualization that the boundary layer only separates from the blade surface at the leading edge of the pressure surface.

Concluding Remarks

The boundary layers on the surfaces of the rotor of a radial inflow turbine have been shown to be laminar/transitional at the design flow condition. This is despite the high value of the surface-length-based Reynolds number. Two reasons have been identified to explain the laminar state of the boundary layer. First, there is significant spanwise secondary flow on the suction surface. As a result the boundary layer on the suction surface moves towards the casing to be replaced by a new boundary layer, which is formed near the hub rather than the leading edge of the blade. Secondly, the large acceleration close to both blade surfaces has the effect of preventing the disturbed laminar boundary layer from becoming fully turbulent.

The velocity ratio across the rotor (at midspan) is higher than the value recommended by Rohlik.[15] This has been achieved mainly as a result of the negative swirl in the stationary frame at the exit from the rotor. It is not clear whether the boundary layers in the turbines designed using similar velocity ratios to those suggested by Rohlik will be laminar. However, the total–total efficiency of this turbine is particularly high ($\eta_{TT} = 0.93 \pm 0.03$), and so it may be a good idea to increase the acceleration in conventional turbines by increasing the velocity ratio. Negative swirl at the rotor exit does, incidentally, have the advantage of increasing the power output from the turbine.

Acknowledgments

The authors would like to acknowledge Rolls–Royce, plc. for their support of the research work. The authors would like to thank S. H. Hill of Rolls–Royce for the design of the high-speed baseline turbine, and J. Saunders of the Whittle Laboratory for his technical assistance during the current program of research.

References

[1]Benson, R. S., Cartwright, W. G., and Jackson, D. C., "Flow Studies in a Low-Speed Radially-Bladed Impeller," *Proceedings of the Institution of Mechanical Engineers*, Vol. 184, 1969–70, Pt. 3G (ii), pp. 30–37.

[2]Ariga, I., Watanabe, I., and Fujie, K., "Investigations Concerning Flow Patterns Within the Impeller Channels of Radial Inflow Turbines, with Some Reference to the Influence of Splitter Vanes," *Journal for Engineering Power*, Vol. 89, Oct. 1967, pp. 463–477.

[3]Kitson, S. T., Maguire, J. M., Langdon, P. J., Varo, R. G., and Shaw, G. D., "The Computational Experiment Applied to Aerodynamic Design and Analysis of Turbomachinery," Society of Automotive Engineers Paper 900360, 1990.

[4]Huntsman, I., and Hodson, H. P., "Measurements and Predictions of the Flow Around the Leading Edge of a Radial Inflow Turbine Rotor," *Tenth International Symposium on Air Breathing Engines*, Vol. 1, 1991, pp. 431–438.

[5]Huntsman, I., Hodson, H. P., and Hill, S. H., "The Design and Testing of a Radial Flow Turbine for Aerodynamic Research," *Journal of Turbomachinery*, Vol. 114, April 1992, pp. 411–418.

[6]Hess, J. L., and Smith, A. M. O., "Calculation of Potential Flow About Arbitrary Bodies," *Progress in Aeronautical Sciences*, 1st ed., Vol. 8, Pergamon, Oxford, England, UK, 1967, pp. 1–138.

[7]Bellhouse, B. J., and Schultz, D. L., "Determination of Mean and Dynamic Skin Friction, Separation and Transition in Low-Speed Flow with a Thin-Film Heated Element," *Journal of Fluid Mechanics*, Vol. 24, No. 2, 1966, pp. 379–400.

[8]Hodson, H. P., "Boundary Layer and Loss Measurements on the Rotor of an Axial Flow Turbine," *Journal of Engineering for Gas Turbines and Power*, Vol. 106, April 1984, pp. 391–399.

[9]Hodson, H. P., "Boundary Layer Transition and Separation near the Leading Edge of a High Speed Turbine Blade," *Journal of Engineering for Gas Turbines and Power*, Vol. 107, Jan. 1985, pp. 127—134.

[10]Denton, J. D., "An Improved Time Marching Method for Turbomachinery Flow Calculation," *Journal of Engineering Power*, Vol. 105, July 1983, pp. 514–524.

[11]Dawes, W. N., "A Numerical Analysis of the Three Dimensional Viscous Flow in a Transonic Compressor Rotor and Comparison with Experiment," American Society of Mechanical Engineers Paper 86-GT-16, 1986.

[12]Wilkinson, D. H., "A Numerical Solution of the Analysis and Design Problems for the Flow Past One or More Aerofoils or Cascades," Aeronautical Research Council R&M 3545, Ministry of Technology, London, 1967.

[13]Wilkinson, D. H., "The Analysis and Design of Blade Shapes for Radial, Mixed and Axial Flow Turbomachines with Incompressible Flow," English Electric Mechanical Engineering Lab. Rept. W/M(3F), 1969, p. 1578.

[14]McFarland, E. R., "A Rapid Blade-Blade Solution for Use in Turbomachinery Design," *Journal of Engineering for Gas Turbines and Power*, Vol. 106, April 1984, pp. 376–382.

[15]Rohlik, H. E., "Radial Inflow Turbines," NASA SP 290, Vol. 3, 1975, Chap. 10.

[16]Herbert, M. V., and Calvert, W. J., "Description of an Integral Method for Boundary Layer Calculation in Use at NGTE, with Special Reference to Compressor Blades," NGTE Memorandum M80219, 1982.

[17]Abu-Ghannan, B. J., and Shaw, R., "Natural Transition of Boundary Layers—The Effects of Turbulence, Pressure Gradient and Flow History," *Journal of Mechanical Engineering Science*, Vol. 22, No. 5, 1980, pp. 213–228.

[18]Hodson, H. P., Addison, J. S., and Sheperdson, C. A., "Models for Unsteady Wake Induced Transition in Axial Turbomachines," *Journal of Physics III*, 1992, pp. 545–574.

[19]Hiett, G. F., and Johnston, I. H., "Experiments Concerning the Aerodynamic Performance of Inward Flow Radial Turbines," *Proceedings of the Institution of Mechanical Engineers*, Vol. 178, Pt. 3I (ii), 1963, pp. 28–42.

[20]Jones, W. P., and Launder, B. E., "Some Properties of Sink Flow Turbulent Boundary Layers," *Journal of Fluid Mechanics*, Vol. 56, Nov. 1972, pp. 337–351.

[21]Mayle, R. E., "The Role of Laminar-Turbulent Transition in Gas Turbine Engines," ASME IGTI Scholar Award Paper, *Journal of Turbomachinery*, Vol. 113, Oct. 1991, pp. 509–537.